Chemistry & Biology
Article

The Development of Peptide-Based Tools for the Analysis of Angiogenesis

Anna Fedorova,[1] Kerry Zobel,[1] Herman S. Gill,[3] Annie Ogasawara,[3] Judith E. Flores,[3] Jeff N. Tinianow,[3] Alexander N. Vanderbilt,[3] Ping Wu,[2] Y. Gloria Meng,[4] Simon-P. Williams,[3] Christian Wiesmann,[5] Jeremy Murray,[2] Jan Marik,[3] and Kurt Deshayes[1,*]
[1]Department of Early Discovery Biochemistry
[2]Department of Structural Biology
[3]Department of Biomedical Imaging
[4]Department of Assay and Automation Technology
Genentech, South San Francisco, CA 94080, USA
[5]Novartis Institutes for BioMedical Research, Novartis Pharma AG, Fabrikstrasse 16, Basel, Switzerland
*Correspondence: deshayes@gene.com
DOI 10.1016/j.chembiol.2011.05.011

SUMMARY

Limitations to the application of molecularly targeted cancer therapies are the inability to accurately match patient with effective treatment and the absence of a prompt readout of posttreatment response. Noninvasive agents that rapidly report vascular endothelial growth factor (VEGF) levels using positron emission tomography (PET) have the potential to enhance anti-angiogenesis therapies. Using phage display, two distinct classes of peptides were identified that bind to VEGF with nanomolar affinity and high selectivity. Co-crystal structures of these different peptide classes demonstrate that both bind to the receptor-binding region of VEGF. ^{18}F-radiolabelling of these peptides facilitated the acquisition of PET images of tumor VEGF levels in a HM7 xenograph model. The images obtained from one 59-residue probe, ^{18}F-Z-3B, 2 hr postinjection are comparable to those obtained with anti-VEGF antibody B20 72 hr postinjection. Furthermore, VEGF levels in growing SKOV3 tumors were followed using ^{18}F-Z-3B as a PET probe with VEGF levels increasing with tumor size.

INTRODUCTION

A promising development in health care is the movement toward targeted therapies that focus treatment on specific biomarkers associated with a particular pathology (van't Veer and Bernards, 2008). Continued advancement in this area will depend on improved diagnostic tools that facilitate not just the customization of treatments for a specific disease, but also the ability to assess the response to these treatments, an approach referred to as evidenced medicine (Basu, 2010). These advances ultimately depend on improved biological understanding of the disease and the molecularly distinct subtypes involved. The significant advances in the understanding of the role of vascular endothelial growth factor (VEGF) in normal and diseased states have made this family of growth factors important targets for therapeutic intervention (Chung et al., 2010). VEGF is a specific mitogen that regulates the formation of new blood vessels during embryogenesis (vasculogenesis) and the sprouting of new blood vessels from pre-existing ones (angiogenesis) (Ferrara and Davis-Smyth, 1997). Anti-VEGF therapies are known to be effective in the treatment of wet macular degeneration (Heier et al., 2006) and cancers such as metastatic colon carcinoma (Hurwitz et al., 2004) and nonsmall cell lung cancer (Sandler et al., 2006), with ongoing efforts underway to identify, expand and improve therapeutic regimens. The levels of VEGF secreted by growing tumor change rapidly in response to increasing hypoxia with VEGF levels correlated with the onset of metastasis (Ferrara and Davis-Smyth, 1997). Molecules that rapidly report tumor VEGF levels in a noninvasive manner would be a valuable tool for managing anti-angiogenesis therapies (Bailey, 2010; Dowlati et al., 2008).

Positron emission tomography (PET) is a clinically used noninvasive imaging technology. Performing PET with radiolabeled antibodies (immunoPET) aspires to be a method of choice for obtaining comprehensive analysis of target expression and availability in vivo (van Dongen et al., 2007). The relatively slow penetration of tracers based on full length antibodies requires uptake periods of 3–6 days to achieve optimum tumor-to-background contrast and the VEGF level can rapidly change during this time in preclinical models (van Dongen et al., 2007). Therefore, an imaging agent based on a smaller scaffold with good tissue permeability allowing more frequent noninvasive sampling of tumor VEGF is warranted. The necessary clearance rate and tissue penetration requires low molecular weight peptides that bind to VEGF with nanomolar affinity that can be modified to give clear PET images using the widely available ^{18}F-radionuclide. For example, numerous accounts were published on in vivo imaging using HER2 specific Z-domain derived peptides with very high tumor uptake values (Kramer-Marek et al., 2008; Orlova et al., 2006). The levels of HER2 receptor in these models are very high (200–1000 ng/mg), for comparison the VEGF amount in the most common models are 100–500 times lower than HER2 levels in a typical HER 3+ tumor and therefore represent a more difficult target for imaging.

VEGF exists as a symmetrical dimer that signals by dimerizing tyrosine kinase receptors, kinase insert domain containing receptor (KDR) or fms-like tyrosine kinase-1 (Flt-1), at two

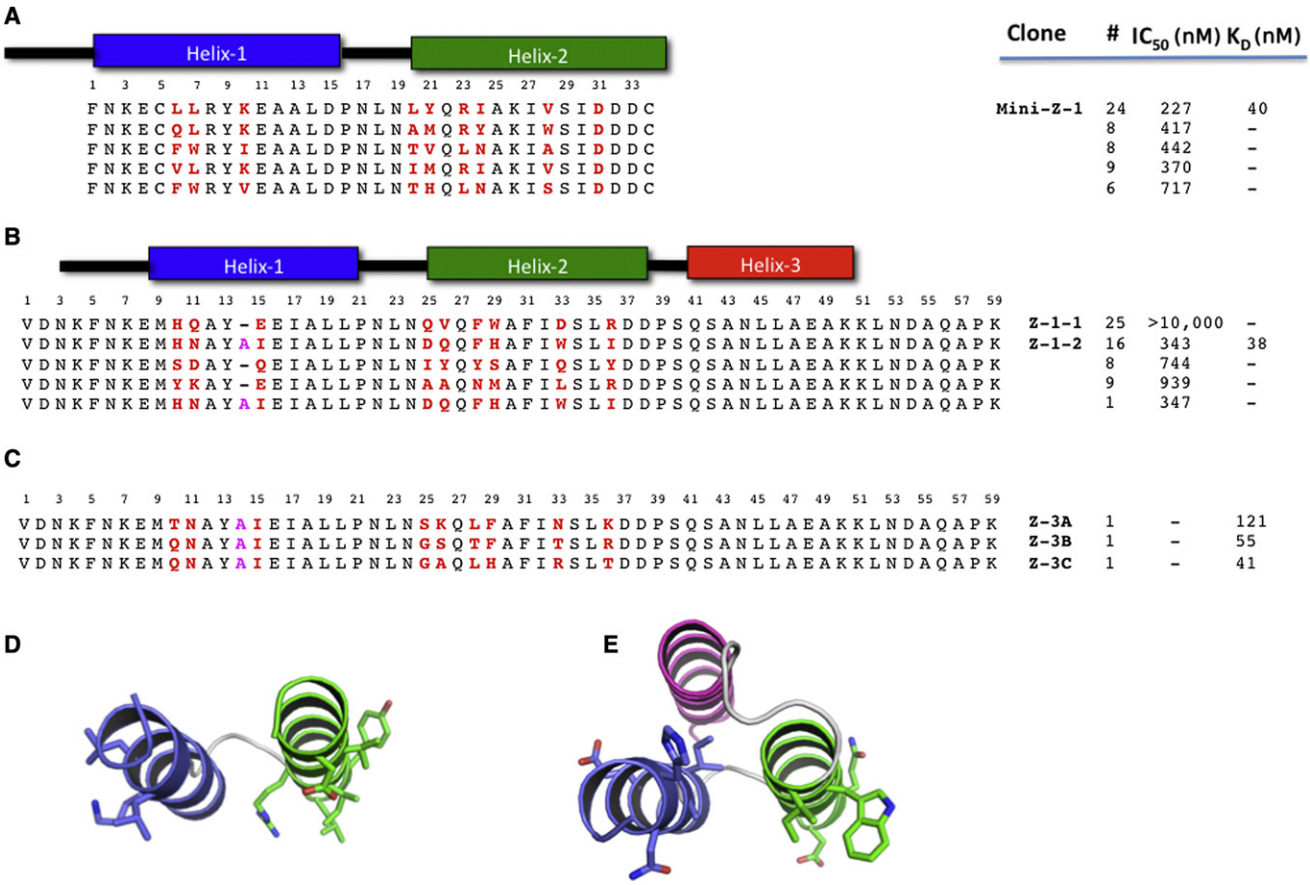

Figure 1. Sequences and VEGF Affinity of Peptides Obtained from Phage Display

(A and B) Dominant peptide sequences identified from the screen against VEGF with first-generation (A) mini-Z and (B) full-length Z-domain libraries.

(C) Tightest peptide binders identified from second-generation full-length Z-domain libraries, with randomized residues shown in red.

(D) Cartoon representation of the crystal structure of the mini-Z highlighting randomized residues shown as sticks and coloring the helices according to (A).

(E) Cartoon representation of the crystal structure of the Z-domain highlighting randomized residues shown as sticks and coloring the helices according to (B).

See also Figures S1 and S2.

identical binding sites located at the poles of the receptor binding domains (Wiesmann et al., 1997). The receptor-binding domain is the most facile binding region as VEGF neutralizing antibodies (Muller et al., 1998), and phage derived peptides bind at this location (Pan et al., 2002; Wiesmann et al., 1998). The peptides derived from the earlier studies (Pan et al., 2002; Wiesmann et al., 1998) are not sufficiently potent to function as effective PET probes. In order to find more potent binders, libraries of a preorganized scaffold were displayed on phage and panned against VEGF. The three helix 58-residue Z-domain of staphylococcal protein A was chosen based on positive results mutating this sequence to recognize the extracellular domain of HER2 (Orlova et al., 2006). Through stabilizing mutations and the addition of a disulfide constraint the Z-domain is reengineered into a two-helix 34-residue "mini-Z" version that retains the parent's affinity (Starovasnik et al., 1997). Both scaffolds can be synthesized using standard solid phase methods in good yield, allowing easy modification for PET imaging applications. We elected to investigate both scaffolds simultaneously by panning libraries displayed on the minor coat protein of M13 phage against $VEGF_{109}$. Here we report on the selection process, describe structural and biochemical characterization of the peptides selected, compare and contrast the image quality obtained from different peptides modified as PET probes in a HM7 colorectal carcinoma xenograft model, and utilize the most promising probe to investigate VEGF levels in a SKOV-3 ovarian cancer xenograft model.

RESULTS

Phage Display

The choice of the nine residues to be randomized was based on previous work reengineering the Z-domain in order to select binders against HER2 (Orlova et al., 2006) (Figure 1). These residues were selected because they define a well organized binding surface within the context of the Z-domain and mini-Z scaffolds (see Structural Studies of VEGF in Complex with Phage-Derived Peptides). Libraries were constructed using standard protocols that contained $>10^9$ unique members (Sidhu et al., 2007) (see Experimental Procedures).

After four rounds of selection with the mini-Z library against $VEGF_{109}$, >95% of the clones bound specifically to VEGF with all clones having unique sequences. After six rounds of selection, clone Mini-Z-1 (FNKECLLRYKEAALDPNLNLYQRIAKIVSI DDDC) dominated (Figure 1A), and proved to be the tightest binder by phage ELISA (IC_{50} ~ 300 nM), with K_d = 40 nM as determined by Octet analysis with the synthetic peptide (see Figure S2A available online). The high affinity of the Mini-Z-1 peptide warranted investigation of its structural and PET imaging properties.

After four rounds of selection with the Z-domain library against $VEGF_{109}$, two unique sequence families were found: Z-1 consisting of 58-residue peptides that aligned with the sequence of the original Z-domain; and a second family, Z-2, in which an extra alanine residue was inserted at position 14. This mutation occurred during the selection process because the original library was constructed exclusively with 58 residue peptides and no 59 residue clone is found when the Z-domain library is sequenced. Both families were present after six rounds, and analysis of the Z-1 clones by phage ELISA showed IC_{50} values approaching the micromolar range (Figure 1). The Z-2 class demonstrated consistently higher affinity for VEGF as determined by phage ELISA (Figure 1). The tightest binding clone from phage ELISA Z-1-2 was confirmed in Octet assay (K_d = 38 nM) with the synthetic peptide (Figure S2B). This is sufficiently potent for PET imaging so Z-1-2 was carried on for structural and PET imaging studies. Phage ELISA assays assessed the selectivity of the mini-Z-1 and Z-1-2 against a panel of targets with neither mini-Z-1 or Z-1-2 showing significant affinity for the extracellular domain of HER2 or IgG, the original targets of the reengineered scaffolds (Figure S1).

Second generation Z-domain libraries explored the role of the additional residue introduced at position 14. Two libraries were constructed that mirrored the original Z-domain libraries but position 14 was randomized to all 20 natural amino acids. Interestingly, all the clones examined after four rounds of sorting contained an alanine at this position, indicating the mutation on phage had selected for the optimal residue. Affinities were determined by competitive phage ELISA, with tightest binders Z-3A, Z-3B, and Z-3C synthesized and K_d values of 121, 55, and 41 nM, respectively, as determined by Octet assay using synthetic peptides (Figure 1). As a control, affinities were obtained by Octet assay for $VEGF_{165}$ and peptide Z-3B and yielded similar results (data not shown). In order to determine total VEGF concentration in mouse xenograft models, the probes should bind comparably to human and murine VEGF. Octet analysis determined that all of the peptides used in PET imaging study bound to both human and murine VEGF with ~2-fold increase in potency for murine VEGF (data not shown).

Structural Studies of VEGF in Complex with Phage-Derived Peptides

We determined the crystal structures of both the Z-1-2 and the mini-Z-1 peptides bound to VEGF at 2.5 Å and 2.9 Å resolution, respectively (see Table S1 for data collection and refinement statistics). The structures revealed that both peptides bind at the two poles of the VEGF homodimer (Figure 2). The overall structure of VEGF does not change on complex formation, and is similar to previously determined VEGF crystal structures

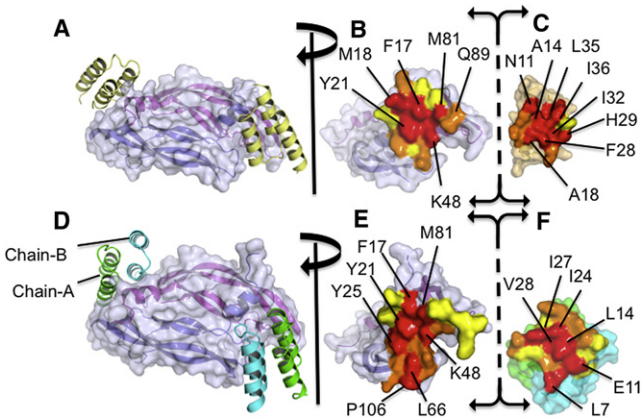

Figure 2. Structures of the Complex between VEGF and the Z-Domain Peptides and VEGF and the Mini-Z Dimer Peptides

(A) Structure of VEGF:Z-domain complex (Protein Data Bank [PDB] code: 3S1K). The VEGF homodimer is rendered as a transparent surface with chains V and W represented as cartoons colored magenta and blue respectively, the Z-domain peptides are represented as a cartoon with chains A and B colored yellow.

(B and C) Open book view of the binding interface between the VEGF dimer and the Z-domain. The VEGF homodimer and the Z-domain are represented as surfaces. Residue coloring symbolizes the extent to which the solvent accessible surface area is buried by complex formation (25%–49%, yellow; 50%–75%, orange; >75%, red).

(D) Structure of the VEGF:mini-Z dimer complex. VEGF is rendered as in (A) and the mini-Z peptides are represented as cartoon with chains A and B of the Z-domain peptide colored green and cyan, respectively.

(E and F) Open book view of the binding interface between the VEGF dimer and the min-Z dimer. The VEGF homodimer and the Z-domain are represented as surfaces. (PDB-ID 3S1K and 3S1B, respectively).

See also Figures S2 and S3 and Table S1.

(Muller et al., 1998; Wiesmann et al., 1997, 1998). The crystal structure of the VEGF:Z-domain complex shows that the Z-domain binds as a three-helix bundle, with two molecules of the Z-domain binding per VEGF dimer. The structure of the VEGF:mini-Z-1 complex revealed that the mini-Z-1 peptides bind to VEGF as dimers with residues from helix-1 of one mini-Z-1 monomer and residues from helix-2 of the other mini-Z-1 monomer forming the VEGF binding interface (Figure S3). The intrachain disulfide bond between Cys5 on helix-1 and Cys34 on helix-2 was well defined by the 2.9 Å electron density. We confirmed that the mini-Z-1 dimer is required for complex formation by mutagenesis of critical residues that are important for the dimerization of mini-Z-1 monomers. We determined that residues that disrupt the mini-Z-1 dimerization interface also bind to VEGF with diminished activity (Figures S2C and S2D). Both the Z-domain and the mini-Z-1 peptides bind to similar locations of the VEGF homodimer and exhibit a high level of surface complementarity for VEGF (Figure 2). Please refer to the Supplemental Experimental Procedures for the description of the interactions between VEGF and mini-Z-1.

There was not sufficient electron density to build the first six residues (VDNKFN) and the last residue (K59) of the Z-domain peptides, suggesting that these residues do not make significant interactions in the crystal structure. The remainder of the Z-domain exhibits electron density and demonstrates that the VEGF binding face of the Z-domain is distributed across helix-1

and helix-2. The interaction of the A-chain and B-chain of the Z-domain peptides with the VEGF dimer are equivalent with minimal differences that are likely due to differences in the crystal environment, and therefore, the crystal structure results will be described using the A-chain of the Z-domain. Of the residues randomized in the selection of Z-domain peptide, Asn11 and His29 are involved in hydrogen bond interactions with residues from both chains V and W of the VEGF dimer. The Nd2 atom of Asn11 makes a hydrogen bond interaction with Oe1 of Gln79 of chain V and the Od1 atom of Asn11 interacts with the backbone NH atom of Met18 that is located in the first turn of helix a1 of chain W. His29, located in helix-2 of the Z-domain, makes important interactions with Tyr21 and Tyr25 that are located at the C terminus of helix a1 of chain W. The Nd1 atom makes a hydrogen bond interaction with the OH atom of Tyr21 whereas the aromatic imidazole ring of His29 stacks on top of the phenol of Tyr25. All the other residues randomized for the selection are involved in complementary van der Waals interactions at the interface between Z-domain helices 1 and 2 and the VEGF dimer, in addition His10 is involved in an intrachain hydrogen bond interaction with the Og atom of Ser41 that is located at the N terminus of helix-3. Other interactions that are likely to aid the binding of the Z-domain to VEGF include a salt bridge interaction between the Od1 atom of Asp26, which is located at the C terminus of helix-1 of the Z-domain, and the Nz atom of Lys48 located on the b2 strand of chain V. The backbone carbonyl of Ala18 at the N terminus of helix-2 is involved in a hydrogen bond interaction with the Ne2 atom of Gln89, located on the b6 strand of chain V.

Both the Z-domain and the mini-Z peptides bind to VEGF at the receptor binding face that is located at the two poles of the homodimer (Figure 2). The Z-domain and mini-Z bind almost entirely across the receptor binding site of VEGF (Wiesmann et al., 1997, 1998). A single Z-domain peptide contacts 14 residues of the VEGF homodimer, with six hydrogen bond interactions and 744 $Å^2$ buried surface area. An interesting result from the initial selections was the insertion of an Ala residue at position 14 of the Z-domain. The Ala14 insertion is located in helix-1 of the Z-domain and the structure suggests it is important as a spacer in helix-1 that shifts the register of the residues in the Z-domain so that they make more optimal interactions with the VEGF homodimer. The side chain of Ala14 is close to the VEGF binding interface, with the Cb atom making favorable van der Waals interactions with the side chain atoms of Met18 in the VEGF dimer. This interaction likely explains why all peptides identified in subsequent rounds of selection retain Ala in this position. Of the other residues randomized in the selection, Asn11 makes two critical interactions with both chains of the VEGF homodimer, the importance of Asn11 is underscored by the results from the selection where it was conserved through rounds of selection. In contrast, although His29 side chain makes a hydrogen bond interaction with Tyr21 of VEGF, this residue was not strongly favored during selection.

PET Imaging Studies

The peptides were ^{18}F-fluorinated by copper catalyzed 1,3-dipolar cycloaddition of 1-[^{18}F]fluoro-11-azido-3,6,9-trioxa undecane (^{18}F-PEG$_4$-N$_3$) to 4-pentynoic acid attached to the N terminus in 21%–45% radiochemical yields within 120 min (see Supplemental Experimental Procedures for details) (Gill et al., 2009). A model of colorectal carcinoma based on the HM7 cell line was used to evaluate the imaging capacity of both the ^{18}F-peptides and ^{89}Zr-radiolabeled anti-VEGF antibody B20 (Liang et al., 2006). This model is known to express relatively high levels of VEGF and the tumor growth is VEGF-dependent. Mice bearing HM7 xenografts on right hind thigh were imaged at 2 weeks after tumor implantation with all tested peptides. In order to minimize the effect of the tumor growth and maximize the throughput, the imaging was performed within 3 consecutive days using low number of animals (n = 1–3) for each peptide. The 120 min dynamic scans were acquired and the peptides were ranked based on tumor uptake, tumor-to-blood and tumor-to-muscle ratios calculated from uptake values summed over the last 30 min of the dynamic scan (Figure S5). The biodistributions of all peptides were similar and were dominated by fast renal and hepatobiliary clearance leading to high uptake in the bladder and intestine. Despite the tumor uptake being only 0.5%–1.0% ID/g, the fast clearance provided low nonspecific uptake in tissues surrounding the tumor, which allowed visualization of the tumor implanted on the right thigh (Figure S4). The uptake of all peptides in the HM7 tumor xenograft was in the same range but ^{18}F-Z-3B provided the best tumor-to-blood and tumor-to-muscle ratios (Figure S5). The tumor uptake of peptide ^{18}F-Z-3B was (0.85 ± 0.14 %ID/g, n = 3) with average tumor-to-blood and tumor-to-muscle ratios equal to 2.2 and 5.6 reached within 2 hr postinjection. The peptide ^{18}F-Z-3B was therefore chosen for further studies.

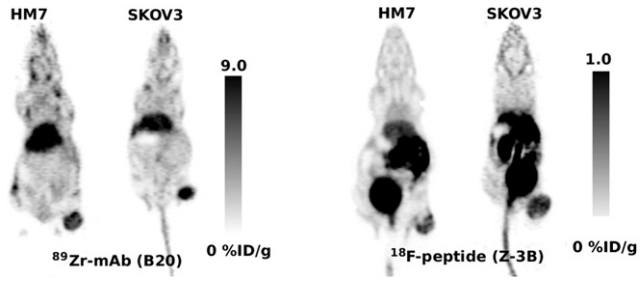

Figure 3. Imaging VEGF in HM7 and SKOV3 Xenografts

Positron emission tomography (PET) images (coronal slice) of mice bearing HM7 xenograft at 2 weeks postimplantation and SKOV3 xenograft at 4 weeks postimplantation obtained with ^{89}Zr-B20 (left) and ^{18}F-Z-3B (right). See also Figures S4 and S5.

Although the tumor uptake of ^{89}Zr-radiolabeled anti-VEGF antibody B20 was approximately eight times higher than tumor uptake of ^{18}F-Z-3B the tumors were clearly visualized by both probes (Figure 3), and the tumor-to-blood and tumor-to-muscle ratios were roughly comparable in HM7 tumor model, 2.3 for antibody 72 hr postinjection and 2.2 for peptide 2 hr postinjection.

The ^{18}F-labeled mini-Z-1 peptide was cleared more rapidly through the renal route than ^{18}F-Z-3B (Figure S7). Concurrent with this work Ren et al. reported a modified mini-Z (Ren et al., 2009) with single digit nanomolar affinity to HER2, with the ^{68}Ga-labeled two-helix peptide showing tumor uptake values only 20% of the three helix Z-domain derived peptide (Orlova et al., 2006). This trend is similar to what we observed with our mini-Z and Z-domain peptides. In light of the superiority of ^{18}F-Z-3B we focused our studies on this imaging agent.

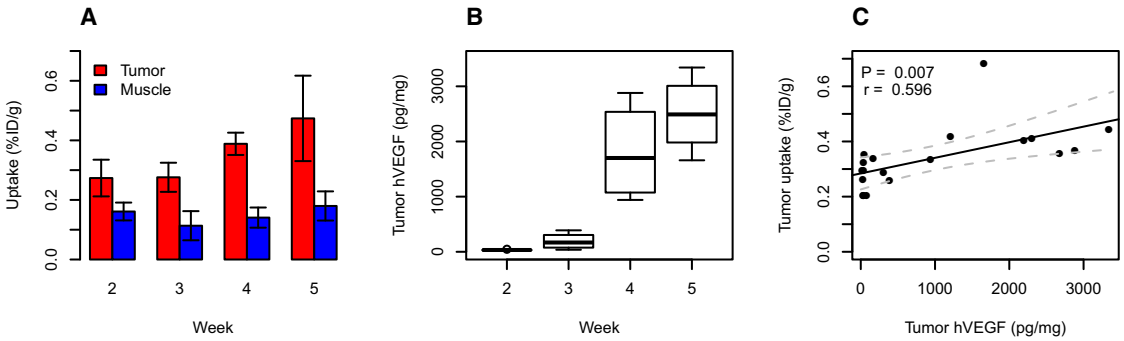

Figure 4. Changes in VEGF Levels

(A and B) The uptake of ^{18}F-Z-3B in SKOV3 xenograft was measured by (A) PET and (B) expression of hVEGF in SKOV3 xenografts was determined ex vivo at 2–5 weeks posttumor implantation.

(C) Correlation of hVEGF amount in the tumor with the uptake of ^{18}F-Z-3B.

See also Figure S6 and S7.

The peptide ^{18}F-Z-3B was used to monitor levels of VEGF in the growing ovarian tumor model based on SKOV3 ovarian cancer cell line. The tumor-to-blood ratios in this model are 2.7 for ^{89}Zr-B20 antibody 72 hr postinjection and 1.4 for the peptide ^{18}F-Z-3B 2 hr postinjection (Figure 3). The VEGF level is known to increase with the tumor size and age as a response to increased hypoxia (Hendriksen et al., 2009). The animals (n = 4–6 per group) bearing SKOV3 tumors were imaged by 30 min static scan after 90 min of conscious uptake at weeks 2, 3, 4, and 5 postinoculation. After imaging, the animals were sacrificed and the tumor tissue was excised and weighted, and the levels of human-VEGF (hVEGF) and murine-VEGF (mVEGF) were measured by ELISA. The tumor uptake of ^{18}F-Z-3B was significantly increased at week 4 compared to weeks 2 and 3 ($p = 0.004$ and 0.005) and remained elevated at week 5 (Figure 4A), which correlated with the increase of hVEGF levels at week 4 compared to weeks 2 and 3 (Figure 4B). The tumors became more heterogeneous presumably due to necrosis as reflected by larger standard deviation at week 5 postinoculation. The tracer uptake in muscle remained unchanged between weeks 2 and 5 (Figure 4A). The levels of mVEGF were 200 times lower than levels hVEGF in the tumor tissue and increased in parallel with levels of hVEGF (Figure S6). The observed increase of the tumor uptake of ^{18}F-Z-3B correlated ($r = 0.60$, $p < 0.01$) with the measured levels of hVEGF (Figure 4C); however, the slope of the regression line is low, and this limits the quantitative prediction of the hVEGF level in the tumor. Hence, although qualitative analysis is feasible, further optimization is needed to develop a reliable quantitative diagnostic.

DISCUSSION

As a first step in developing peptide-based diagnostics that rapidly and reliably monitor tumor VEGF levels, we have used phage display to identify novel 34-residue two-helix and 59-residue three-helix domain peptides based on the Z-domain of protein A. In the case of the 59-residue peptide we discovered that only peptides incorporating an extra alanine into helix 1 bound to VEGF with detectable affinity. Analysis of the crystal structure of the complex between VEGF and the Z-domain peptide suggests a change in helix register is responsible for increased binding affinity over the 58-residue peptide. Another unanticipated result is that dimerization of 34-residue mini-Z peptide is required for VEGF recognition. The combinatorial biology approach used in this study was crucial in the identification of two new classes of VEGF binding peptides, pointing to the utility of this approach for obtaining novel high affinity binding scaffolds to important biological targets (Sidhu et al., 2003).

A limiting factor in the application of PET imaging as a method to monitor therapeutic regiment is the lack of suitable probes that monitor disease state in a clinically relevant time frame. The importance of anti-angiogenesis therapies suggest that monitoring tumor VEGF levels in real time will be a critical tool for maximizing patient benefit. This study demonstrates that peptides can be used to detect VEGF in animal models. The PET images obtained with the ^{18}F-labeled 34-residue mini-Z peptides showed poor tissue penetration and rapid renal clearance, which yielded tumor to tissue ratios insufficient for the production of usable images. However, the 59-residue peptide, Z-3B, when radio-labeled with ^{18}F yields PET images of tumor VEGF levels 2 hr postinjection that are comparable to those obtained with ^{89}Zr-radiolabeled anti-VEGF antibody 72 hr postinjection. The ^{18}F-labeled Z-3B is suitable for quantitative determination of local VEGF level, demonstrating that it is possible to use peptide-based tracers to image VEGF levels in a widely accepted whole animal cancer model. We feel this is an important step in creating new diagnostics that will guide anti-angiogenesis therapeutics by identifying the optimal dosing regiment and drug combinations that achieve the best patient outcome. Work to optimize the system to produce images that better quantitate tumor VEGF levels is under way and will be reported in due course. The further optimization shall include increasing the binding affinity and avidity (Friedman et al., 2007) of the peptide as well as optimizing its clearance and metabolism.

SIGNIFICANCE

The implementation of target-based therapy and evidence based medicine require the development of sensitive diagnostics that allow physicians to assess patient response to

treatment and customize each individuals therapy accordingly. An attractive diagnostic approach in cancer is the use of positron emission tomography (PET) to obtain rapid images of how tumors are responding to treatment. PET probes for tumor metabolism and proliferation are already in clinical use. Antibody based probe has been developed to investigate tumor vascularization by targeting vascular endothelial growth factor (VEGF). However, it is preferable to obtain high quality images in a single clinical visit as opposed to having to wait days between PET probe introduction and the opportunity to obtain high contrast images as required with antibody based probes. In addition to convenience, the use of short half-life isotopes also reduces the overall radiation burden, making repeat measurements more attractive. In order to create probes that image VEGF two classes of peptides derived from the Z-domain of protein A were developed that selectively bound to VEGF with nanomolar affinity, with recognition at the receptor binding site as demonstrated by X-ray crystal structure analysis. The smaller 38-residue peptide binds to VEGF as a dimer and did not yield images with contrast comparable to those obtained with antibody based probes. However, one 59-residue three helix ^{18}F-labeled peptide produces images 2 hr postinjection that are comparable to images obtained 72 hr postinjection with an ^{89}Zr-labeled anti-VEGF antibody. These results are a proof of concept for rapidly imaging tumors by binding to an angiogenesis factor, which can potentially serve as reporters of the effects of anti-angiogenesis therapies.

EXPERIMENTAL PROCEDURES

Phage Panning and Analysis

N-terminal gene 3 minor coat protein-displayed peptide libraries (>10^9 unique members) were constructed by previously described methods (Sidhu et al., 2007). Randomization of desired positions was done using trinucleotide chemistry that allowed incorporation of 17 natural amino acids (Cys, Pro, and Gly were excluded). For second generation libraries, NNK degenerate codons were used (N = A/G/C/T and K = G/C) to allow randomization with all 20 natural amino acids (see Supplemental Experimental Procedures for details of the selection, peptide synthesis, and Octet analysis).

Peptide Synthesis

Peptide were synthesized on The Symphony (Protein Technologies). Standard Fmoc chemistry was used for the syntheses and each amino acid was double coupled using HBTU, *O*-Benzotriazole-*N,N,N′,N′*-tetramethyl-uronium-hexafluorophosphate, as the peptide coupling reagent. The peptides were taken off the instrument and cleaved manually with 95% trifluoroacetic acid, 2.5% triisopropylsilane, and 2.5% water for 2 hr. All peptides with two cysteine residues were cyclized by adding concentrated iodide in acetic acid to the crude peptide. The mixture was stirred for 5 min followed by addition of Zn dust to quench the excess of iodide. The crude peptides were then filtered through celite. The peptides were purified by preparative high performance liquid chromatography. Biotinylated peptides were synthesized as described above on The Symphony. A linker was coupled to the peptide before biotinylation. On removal from the instrument the peptide on resin was reacted with a solution of Fmoc-6-aminohexanoic acid (three equivalents), HATU, (2-(7-Aza-1H-benzotriazole-1-yl)-1,1,3,3-tetramethyluronium hexafluorophosphate), (three equivalents), and diisopropylethylamine (five equivalents) in DMF for 20 min. The Fmoc protecting group was removed with 20% piperidine in DMF for 5 min. Biotin (three equivalents) was then coupled to the peptide in a solution of DMF with a 1 M solution of *N,N′*-Diisopropylcarbodiimide in dichloromethane (three equivalents) for 24 hr. The peptides were cleaved, cyclized, and purified as described above.

Structural Analysis

Residues 8–109 of $VEGF_{109}$ were expressed, refolded, and purified as previously described (Christinger et al., 1996) and buffer-exchanged into 20 mM Tris, pH 7.5, 150 mM NaCl. Both Mini-Z-1 and Z-2 were synthesized by solid-phase methods and acetylated at the N terminus. Both peptides were dissolved in 20 mM Tris, pH 7.5, 150 mM NaCl, mixed with $VEGF_{109}$ in a 3:1 molar ratio, after which the mixture was equilibrated on ice for ~1.5 hr and used in crystallization trials without further purification. The $VEGF_{109}$ concentration in final mixture was optimized to 6 mg/ml.

Crystallization screening of the $VEGF_{109}$:Mini-Z-1 complex resulted in crystals growing in 0.1 M NaOAc, 0.02 M $CaCl_2$, MPD 30.0% v/v, pH 6.0. Crystals were optimized by microseeding into hanging drops composed of a mixture of 2 μl complex and 2 μl reservoir solution (83 mM NaOAc, 17 mM $CaCl_2$, MPD 25.0% v/v, pH 6.0). The crystals were cryoprotected, flash frozen in liquid nitrogen and diffraction data were collected at ALS Beamline 5.0.2 . The $VEGF_{109}$:Z-2 complex crystals grew from 0.2 M KI, 0.1 M MES, PEG 4000 25.0% v/v, pH 6.5. The crystals were cryoprotected, flash frozen in liquid nitrogen, and diffraction data collected at ALS Beamline 5.0.2.

Radiochemical Synthesis

^{18}F-peptides were prepared according to a previously published procedure (Gill et al., 2009). Synthetic details are given in the Supplemental Experimental Procedures along with the preparation of the ^{89}Zr-antiVEGF antibody.

Animal Models

NCR nude mice of 8–10 weeks of age were obtained from Taconic and athymic nude mice 8–10 weeks of age were purchased from Harlan Sprague Dawley (Livermore, CA). Mice were inoculated on the right thigh with 5 × 10^6 SKOV3 cells (NCR nude) or 3.5 × 10^6 HM7 cells (athymic nude) in 100 ml of Hank's buffered salt solution. The athymic nude mice were Animal care and treatment followed protocols approved by Genentech Institutional Animal Care and Use Committee that is accredited by the Association for Assessment and Accreditation of Laboratory Animal Care.

MicroPET Imaging

Mice were anesthetized with ~3% sevoflurane to effect and injected intravenously via the tail vein with 0.2–0.3 mCi of ^{18}F-radiolabeled peptide in isotonic solution or 0.1–0.2 mCi of ^{89}Zr-radiolabeled mAb (100–130 mL). The PET imaging was performed on an Inveon PET/CT scanner. Animals were placed head-first, prone position on the scanner bed and static or dynamic scans were acquired. For ^{18}F-peptides, dynamic data were acquired for 0–120 min posttracer injection; alternatively, 30 min static scan was performed after 90 min of conscious uptake period. For ^{89}Zr-mAb, static 30 min data were collected at day 5 posttracer injection. Body temperature was measured by a rectal probe and maintained with warm air. Full-body iterative image reconstructions were obtained using maximum a posteriori algorithm (MAP, hyperparameter β = 0.05) and corrected for signal attenuation using the tissue density obtained from CT. Projections were created with ASIPro software (Siemens Preclinical Solutions) and used to obtain quantitative activity levels in each organ of interest using region-of-interest analysis. The animals were sacrificed immediately after imaging and tumors were collected, weighed, and subjected to analysis of VEGF levels.

VEGF Level Measurement

The ELISA for VEGF protein in tumor was performed as previously described with minor modifications (Liang et al., 2006). Briefly, excised tumor was homogenized in 500 ml RIPA buffer (Sigma) and, after centrifugation, supernatant was collected and measured for total protein concentration by BCA assay (Pierce). For human-VEGF (hVEGF), a sandwich ELISA was performed using mAb 3.5F8 as coat and biotinylated A4.6.1 as detection antibody. A standard curve was generated using 1–128 pg/mL of $hVEGF_{165}$. For murine-VEGF (mVEGF), a goat anti-mVEGF antibody (R&D Systems) coat and biotinylated goat anti-mVEGF detection antibody was used. A standard curve was generated using 1–128 pg/mL of $mVEGF_{164}$ (R&D Systems). To account for variable

protein extraction efficiency from tumor tissue, measured VEGF levels were normalized to the total protein concentration.

Statistical Analysis

The plots were constructed with R software version 2.10.1 (R Foundation for Statistical Computing, Vienna, Austria). Statistical significance was determined using a two-tailed Student's t test or analysis of variance and p values < 0.05 were considered significant; data are presented as mean ± standard deviation if not stated otherwise.

SUPPLEMENTAL INFORMATION

Supplemental Information includes Supplemental Experimental Procedures, seven figures, and one table and can be found with this article online at doi:10.1016/j.chembiol.2011.05.011.

ACKNOWLEDGMENTS

The authors would like to thank Betty Li for help with cloning, Dev Sidhu and Charlie Eigenbrot for helpful discussion, Jean-Michel Vernes for VEGF expression analysis, and the Genentech DNA synthesis group for providing oligonucleotides. All authors are or have been employees of Genentech., Inc.

Received: March 9, 2011
Revised: April 26, 2011
Accepted: May 2, 2011
Published: July 28, 2011

REFERENCES

Bailey, R.C. (2010). Grand challenge commentary: informative diagnostics for personalized medicine. Nat. Chem. Biol. *6*, 857–859.

Basu, S. (2010). Personalized versus evidence-based medicine with PET-based imaging. Nat. Rev. Clin. Oncol. *7*, 665–668.

Christinger, H.W., Muller, Y.A., Berleau, L.T., Keyt, B.A., Cunningham, B.C., Ferrara, N., and de Vos, A.M. (1996). Crystallization of the receptor binding domain of vascular endothelial growth factor. Proteins *26*, 353–357.

Chung, A.S., Lee, J., and Ferrara, N. (2010). Targeting the tumour vasculature: insights from physiological angiogenesis. Nat. Rev. Cancer *10*, 505–514.

Dowlati, A., Gray, R., Sandler, A.B., Schiller, J.H., and Johnson, D.H. (2008). Cell adhesion molecules, vascular endothelial growth factor, and basic fibroblast growth factor in patients with non-small cell lung cancer treated with chemotherapy with or without bevacizumab—an Eastern Cooperative Oncology Group Study. Clin. Cancer Res. *14*, 1407–1412.

Ferrara, N., and Davis-Smyth, T. (1997). The biology of vascular endothelial growth factor. Endocr. Rev. *18*, 4–25.

Friedman, M., Nordberg, E., Höidén-Guthenberg, I., Brismar, H., Adams, G.P., Nilsson, F.Y., Carlsson, J., and Ståhl, S. (2007). Phage display selection of Affibody molecules with specific binding to the extracellular domain of the epidermal growth factor receptor. Protein Eng. Des. Sel. *20*, 189–199.

Gill, H.S., Tinianow, J.N., Ogasawara, A., Flores, J.E., Vanderbilt, A.N., Raab, H., Scheer, J.M., Vandlen, R., Williams, S.P., and Marik, J. (2009). A modular platform for the rapid site-specific radiolabeling of proteins with ^{18}F exemplified by quantitative positron emission tomography of human epidermal growth factor receptor 2. J. Med. Chem. *52*, 5816–5825.

Heier, J.S., Antoszyk, A.N., Pavan, P.R., Leff, S.R., Rosenfeld, P.J., Ciulla, T.A., Dreyer, R.F., Gentile, R.C., Sy, J.P., Hantsbarger, G., and Shams, N. (2006). Ranibizumab for treatment of neovascular age-related macular degeneration: a phase I/II multicenter, controlled, multidose study. Ophthalmology *113*, 633.e631–633.e634.

Hendriksen, E.M., Span, P.N., Schuuring, J., Peters, J.P., Sweep, F.C., van der Kogel, A.J., and Bussink, J. (2009). Angiogenesis, hypoxia and VEGF expression during tumour growth in a human xenograft tumour model. Microvasc. Res. *77*, 96–103.

Hurwitz, H., Fehrenbacher, L., Novotny, W., Cartwright, T., Hainsworth, J., Heim, W., Berlin, J., Baron, A., Griffing, S., Holmgren, E., et al. (2004). Bevacizumab plus irinotecan, fluorouracil, and leucovorin for metastatic colorectal cancer. N. Engl. J. Med. *350*, 2335–2342.

Kramer-Marek, G., Kiesewetter, D.O., Martiniova, L., Jagoda, E., Lee, S.B., and Capala, J. (2008). [^{18}F]FBEM-Z(HER2:342)-Affibody molecule—a new molecular tracer for in vivo monitoring of HER2 expression by positron emission tomography. Eur. J. Nucl. Med. Mol. Imaging *35*, 1008–1018.

Liang, W.C., Wu, X., Peale, F.V., Lee, C.V., Meng, Y.G., Gutierrez, J., Fu, L., Malik, A.K., Gerber, H.P., Ferrara, N., and Fuh, G. (2006). Cross-species vascular endothelial growth factor (VEGF)-blocking antibodies completely inhibit the growth of human tumor xenografts and measure the contribution of stromal VEGF. J. Biol. Chem. *281*, 951–961.

Muller, Y.A., Chen, Y., Christinger, H.W., Li, B., Cunningham, B.C., Lowman, H.B., and de Vos, A.M. (1998). VEGF and the Fab fragment of a humanized neutralizing antibody: crystal structure of the complex at 2.4 A resolution and mutational analysis of the interface. Structure *6*, 1153–1167.

Orlova, A., Magnusson, M., Eriksson, T.L., Nilsson, M., Larsson, B., Höidén-Guthenberg, I., Widström, C., Carlsson, J., Tolmachev, V., Ståhl, S., and Nilsson, F.Y. (2006). Tumor imaging using a picomolar affinity HER2 binding Affibody molecule. Cancer Res. *66*, 4339–4348.

Pan, B., Li, B., Russell, S.J., Tom, J.Y., Cochran, A.G., and Fairbrother, W.J. (2002). Solution structure of a phage-derived peptide antagonist in complex with vascular endothelial growth factor. J. Mol. Biol. *316*, 769–787.

Ren, G., Zhang, R., Liu, Z., Webster, J.M., Miao, Z., Gambhir, S.S., Syud, F.A., and Cheng, Z. (2009). A 2-helix small protein labeled with ^{68}Ga for PET imaging of HER2 expression. J. Nucl. Med. *50*, 1492–1499.

Sandler, A., Gray, R., Perry, M.C., Brahmer, J., Schiller, J.H., Dowlati, A., Lilenbaum, R., and Johnson, D.H. (2006). Paclitaxel-carboplatin alone or with bevacizumab for non-small-cell lung cancer. N. Engl. J. Med. *355*, 2542–2550.

Sidhu, S.S., Fairbrother, W.J., and Deshayes, K. (2003). Exploring protein-protein interactions with phage display. ChemBioChem *4*, 14–25.

Sidhu, S.S., Feld, B.K., and Weiss, G.A. (2007). M13 bacteriophage coat proteins engineered for improved phage display. Methods Mol. Biol. *352*, 205–219.

Starovasnik, M.A., Braisted, A.C., and Wells, J.A. (1997). Structural mimicry of a native protein by a minimized binding domain. Proc. Natl. Acad. Sci. USA *94*, 10080–10085.

van Dongen, G.A., Visser, G.W., Lub-de Hooge, M.N., de Vries, E.G., and Perk, L.R. (2007). Immuno-PET: a navigator in monoclonal antibody development and applications. Oncologist *12*, 1379–1389.

van't Veer, L.J., and Bernards, R. (2008). Enabling personalized cancer medicine through analysis of gene-expression patterns. Nature *452*, 564–570.

Wiesmann, C., Christinger, H.W., Cochran, A.G., Cunningham, B.C., Fairbrother, W.J., Keenan, C.J., Meng, G., and de Vos, A.M. (1998). Crystal structure of the complex between VEGF and a receptor-blocking peptide. Biochemistry *37*, 17765–17772.

Wiesmann, C., Fuh, G., Christinger, H.W., Eigenbrot, C., Wells, J.A., and de Vos, A.M. (1997). Crystal structure at 1.7 A resolution of VEGF in complex with domain 2 of the Flt-1 receptor. Cell *91*, 695–704.